Effects of nitrogen-containing functional groups of reduced graphene oxide as a support for Pd in selective hydrogenation of cinnamaldehyde

Reza Khaleghi Abasabadi[1] · Abbas Ali Khodadadi[1] · Yadollah Mortazavi[1]

Abstract

The importance of electronic and chemical properties of nitrogen-doped reduced graphene oxide (NRGO) has attracted more attention in recent years. Various carbon–nitrogen bonds with different chemical properties are formed in the process of nitrogen doping (N-doping) of reduced graphene oxide, such as pyrrolic-N, pyridinic-N, and graphitic-N. These types of carbon–nitrogen bonds in the structure are distinctly effective when they are used as catalyst support. This study reveals that various types of carbon–nitrogen bonds of the support affect activity and selectivity of hydrogenation of cinnamaldehyde to hydrocinnamaldehyde reaction differently by palladium active phase. The catalyst supports were synthesized with thermal treatment at three different heat treatment and atmosphere procedures, i.e., 500 and 900 °C, in the presence of ammonia diluted with argon. Various procedures led to different types of carbon–nitrogen bond and different quantity of nitrogen doping of the support. Following the support synthesis, palladium active phase was deposited on the support by an incipient wetness impregnation method. The catalysts were characterized by ICP-OES, XPS, elemental analysis, Raman spectroscopy, FESEM, BET, TPD, TPR, CO chemisorption, and HRTEM. The characterization results showed that Pd dispersion and its size distribution were affected by the quantity and the type of carbon–nitrogen species of the support. The pyridinic nitrogen, as electron acceptor species, seems to have a positive impact on a more uniform distribution of Pd. The catalytic activity was evaluated in a high-pressure bubble column reactor. In this work, the catalyst containing 4.5 wt% Pd supported on NRGO with 2.4% nitrogen and treated at 500 °C showed a maximum conversion of about 98% with high selectivity (96%) for the reaction.

Keywords Reduced graphene oxide · N-doping · Palladium · Cinnamaldehyde · Hydrogenation

✉ Yadollah Mortazavi
   mortazav@ut.ac.ir

1   Catalysis and Nanostructured Materials Research Laboratory, School of Chemical Engineering, College of Engineering, University of Tehran, P.O. Box 11155/4563, Tehran, Iran

Introduction

Selective hydrogenation of α, β-unsaturated aldehydes is one of the most critical and challenging reactions among the research groups both in academia and industries [1, 2]. Cinnamaldehyde (CMA) hydrogenation is reported as a typical model for selective hydrogenation of C=C and C=O [3]. In recent years, many studies have reported that CMA hydrogenation produces fine chemicals using various catalysts under different conditions [4]. Hydrogenation of C=C to produce hydrocinnamaldehyde (HCMA) is an essential process in the pharmaceutical industries, especially producing HIV medicine [5]. The main goal in the reaction is to achieve a high selectivity of the desired product, i.e., HCMA [6].

Several factors, such as supports properties, the electronic and surface chemistry, the nature of the metallic phases, and size of metal active phase, can significantly affect the catalytic performance. Therefore, choosing a suitable metal, support, and a proper synthesis method can considerably increase both activity and selectivity of the reaction [6, 7]. Many noble metals have been used as active phases to activate the double bonds in CMA. The selectivity of the reaction has been studied by various research groups using different metals. It has been shown that the selectivity of metal active phase for hydrogenation of C=C bond toward formation of HCMA follows the sequence of Os < Ir < Pt < Ru < Pd. Palladium catalyst is recognized as the most prevalent metal in this process [8, 9]. Furthermore, supports with increased specific surface area and appropriate dispersion of the active metal play a vital role in the activity and selectivity of hydrogenation, which is related to the interaction between the metal particles and the support [10, 11].

Graphene is considered as a suitable supporting substance for noble metal catalysts owing to its two-dimensional nanosheet structure. Presenting a large surface area, high electric conductivity, and high mechanical strength make it a proper candidate for dispersion of metal nanoparticles [12]. Nevertheless, weak interaction between graphene and metal may lead to less-uniform dispersion of metal active sites and aggregation of metal particles which in turn results in weak catalytic performance in the course of reaction [13]. Therefore, some factors related to the structure of graphene may be tuned in such a way that the metal–support interaction modified. Nitrogen doping (N-doping) is considered one of the feasible routes for modification of graphene properties. This route has received more attention in recent studies [14, 15]. N-graphene is not the same as pristine graphene with respect to different properties. The nitrogen-containing functional groups can take part in catalytic reactions, including the oxygen reduction reaction or anchoring the metal nanoparticles used in the catalytic reaction [16, 17]. The usual bonding of N-doping in a specific carbon matrix includes pyrrolic-N, pyridinic-N, and graphitic-N forms. Graphitic-N atoms substitute carbon atoms in carbon planes, while pyridinic-N atoms are situated at the edges in vacant spaces of the graphitic carbon layers, and pyrrolic-N atoms are placed in the pentagonal ring structures [18, 19].

In the present study, Pd nanoparticles were prepared through an incipient wetness impregnation method and were immobilized onto nitrogen-doped reduced

graphene oxide (NRGO), which was synthesized by a common source of nitrogen, namely ammonia (NH_3), and tested for the selective hydrogenation of CMA. The results of this study demonstrate the effects of N species on dispersion of the metal and consequently on catalytic performance, i.e., activity and selectivity, for this hydrogenation reaction.

Experiments

Materials

Materials including graphite microparticles (< 50 μm), sulfuric acid (98%), phosphoric acid (85%), potassium permanganate (98%), hydrogen peroxide (30%), hydrochloric acid (37%), ethanol (99.9%), palladium (II) chloride (99%), sodium borohydride (96%), cyclohexane (99%), and cinnamaldehyde (95%) were purchased from Merck (Darmstadt, Germany).

Catalyst preparation

Supports synthesis

According to the improved hummers' method for preparing graphene oxide (GO) [20], a mixture of concentrated $H_2SO_4:H_3PO_4$ (45:5 mL) was added to a mixture of graphite flakes (1.0 g) and $KMnO_4$ (6.0 g). First, the reaction temperature was increased to 40 °C, and the mixture was stirred for 48 h. Afterward, it was cooled down, and 10% H_2O_2 was added dropwise at ice bath temperature. The mixture was then centrifuged (4500 rpm for 4 h), and the supernatant liquid was discarded. Then, 400 mL of deionized water and 50 mL of ethanol were used consecutively to wash the pellet. The vacuum drying process was carried out on the collected solid on the filter at 40 °C, yielding 1.7 g of the product.

According to the Staudenmaier method to prepare reduced graphene oxide (RGO), thermal expansion was applied to synthesize RGO followed by the heat treatment at 600 °C for 30 s [21]. NRGO was synthesized by exposing RGO to high-purity ammonia diluted with argon (10% NH_3/Ar) at 500 °C (NRGO500) and 900 °C (NRGO900) for 2 h followed by cooling to room temperature, by disconnecting the heating source and under argon atmosphere. Annealing NRGO900 (ANRGO900) sample was obtained with the same procedure used for NRGO900 sample except the annealing step under argon atmosphere at 900 °C for 4 more hours.

Deposition of Pd on the support

First, 300 mg of the support and 300 mL of deionized water were mixed in a beaker and were further sonicated for 15 min (support slurry). Moreover, the solution of H_2PdCl_4 (4 mM) was prepared by dissolving 35.4 mg $PdCl_2$ in 50 mL of 8 mM HCL in a water bath at 70 °C. Then, 37 mL of H_2PdCl_4 solution was added to the

support slurry at ice bath temperature, and the resultant mixture was later subjected to the ultrasonic probe (100 W) for 15 min [22]. NaBH$_4$ solution (C$=$1 mg/mL) was then added in order to reduce and deposit the Pd-containing slurry in the form of metallic Pd nanoparticles on the supports. Eventually, the catalyst was filtered, washed with deionized water several times, and dried at 70 °C overnight. Inductively coupled plasma optical emission spectrometry (ICP-OES, VISTA-PRO, Australia) was used to measure the loading amount of Pd on NRGO equaled 4.5 wt%.

Catalyst characterizations

The specific surface areas of the samples were determined by Brunauer–Emmett–Teller (BET) method using a CHEMBET-3000 device. The morphology of support was observed by field emission scanning electron microscopy (FESEM) on an FEI Nova NanoSEM 450. High-resolution transmission electron microscope (HRTEM) was used in an FEI Tecnai G2 F20 working at 200 kV. The sample was prepared by adding catalyst solution dropwise to 2-propanol on a copper-coated carbon TEM grid. To obtain the particle size distribution and estimate the average particle size, at least 150 particles were manually measured. The palladium loading in the catalysts was determined by an inductively coupled plasma optical emission spectrometry (ICP-OES, VISTA-PRO, Australia). The amount of nitrogen in the support structure was measured by an elemental analysis system (Eager 300 for EA1112). The X-ray photoelectron spectroscopy (XPS) was performed by a Gamma data-scienta ESCA200 hemispherical analyzer equipped with an AlK$_\alpha$ X-ray source (1486.6 eV). The Raman spectra were obtained on a Texan Raman spectrometer by DPSS Nd:YAG (W) laser.

The temperature-programmed desorption (TPD) technique was employed to measure the oxygen-containing groups on the surface of NRGO samples. First, 50 mg of the sample was degassed at 100 °C for 1 h under 20 mL/min of helium flow and let to cool. Then, TPD was performed starting from 50 up to 1000 °C at a ramp rate of 10 °C/min under 20 mL/min of helium flow. The desorbed gases were analyzed using an online Fourier transform infrared (FTIR) instrument.

Pulsed carbon monoxide chemisorption was performed to measure the dispersion of Pd on the support surface. Prior to chemisorption experiments, the following steps were taken;

(1) the samples were degassed at 100 °C by 20 mL/min of O$_2$ trapped-purified Ar and let to cool to room temperature,

(2) the degassed samples were heated from room temperature to 250 °C for 2 h under 20 mL/min of hydrogen flow to ensure the metallic state of palladium, let to cool to 100 °C under hydrogen flow, and cool to room temperature under 20 mL/min of O$_2$ trapped-purified Ar,

(3) subsequently, the sample treated as such was exposed to consecutive pulses of 0.2 mL 5.0 vol% of CO in Ar mixture and the effluent from the chemisorption rector was analyzed.

To analyze the effluent of the chemisorption reactor continuously and accurately, a flame ionization detector (FID) was used. Prior to FID, a methanizer was used to convert carbon monoxide to methane in order to be detected and measured by FID which is much more sensitive than the thermal conductivity detector (TCD).

The temperature-programmed reduction (TPR) tests were conducted on 15 mg of the samples under 8 mL/min of 7.0% H_2 in Ar. Before reduction, samples were degassed in 10 mL/min N_2 flow at 100 °C for 2 h and left to cool. In the last step, the temperature was increased from 50 to 1000 °C with a heating rate of 10 °C/min.

Catalyst testing

The selective hydrogenation of CMA, leading to the production of the major products of HCMA, cinnamyl alcohol (CMO), and hydrocinnamyl alcohol (HCMO), has been investigated in comparison with the graphene supported Pd catalysts. Hydrogenation reaction was performed in a 50 mL stainless Bubble Column Reactor. 50 mg of catalysts was reduced under H_2 flow (20 mL/min) at 250 °C for 2 h. Catalytic reaction was performed with 0.5 mL (4 mmol) of CMA added to 20 mL of cyclohexane (constant CAL primary concentration of 0.2 mol/L) [23]. The reactor was first pressurized with H_2 up to 2 Mpa and then heated up to 90 °C. The reaction took place at these conditions for 1 h. After that, the heating source was disconnected and let it cool to room temperature which was then followed by depressurizing the reactor.

Gas chromatography (PerkinElmer 8410) was used to analyze the effluent of the reactor. The GC analyzer consisted of the following parts: FID detector, 1.5 m, and 2.2 mm ID column packed with SE-30 on 25/100 Chromosorb P [24]. For the evaluation of catalytic activity and selectivity to HCMA [25], the following parameters were calculated according to Eqs. (1) and (2):

$$\text{CAL conversion(mol\%)} = \frac{n_{CAL_{in}} - n_{CAL_{out}}}{n_{CAL_{in}}} \times 100 \tag{1}$$

$$\text{Selectivity to HCMA(mol\%)} = \frac{n_{HCAL_{out}}}{n_{CAL_{in}} - n_{CAL_{out}}} \times 100 \tag{2}$$

Also, the reaction rates were measured at lower CMA conversions (reacting in a short time) in order to avoid a noticeable change in the reactant concentration. At these conditions, turnover frequency (TOF) was calculated according to the following equation:

$$\text{TOF} = \frac{n_{conv}}{n_M \times t} \tag{3}$$

where n_M is the number of moles of the active sites measured by CO chemisorption, n_{conv} is the number of moles of CAL converted, and t is the reaction time in second.

The catalyst reusability was evaluated using the following procedure: after the reaction was stopped, the reactor was cooled to room temperature and then

depressurized, and the catalyst was collected carefully, drained, washed with acetone 3 times, and dried at ambient temperature. Finally, the next batch of the reaction was performed with the catalyst prepared as such. This procedure was repeated 4 times.

Results and discussion

Structural characterization of the supports and Pd-containing samples

Elemental analysis

The nitrogen-containing functional groups of the catalyst were determined by elemental analysis (Table 1). N-doping at different temperatures showed that NRGO500 sample had lower nitrogen content than the NRGO900 sample; thus, nitrogen doping at higher temperature led to the formation of higher nitrogen-containing functional groups. Due to the reduction of GO and the removal of more oxygen-containing groups, the N-doping process at 900 °C results in more carbon–oxygen or carbon–carbon bonds to break as compared to N-doping at 500 °C, suggesting more nitrogen replacement are more likely [26].

In addition, nitrogen content in the ANRGO900 decreased from 4.4 to 1.5% due to longer exposure, i.e., 4 h, of NRGO900 to 900 °C. According to the previous studies, pyrrolic-N and pyridinic-N are removed or converted to more stable nitrogens (graphitic-N) in the process, i.e., the nitrogen bonds are broken and combined with residual oxygen-containing groups [27]. Therefore, by performing various treatment on graphene oxide, three types of NRGO with different types of nitrogen species (pyrrolic, pyridinic, and graphitic types nitrogen) are synthesized. These samples along with the RGO were considered for further investigation.

N$_2$ adsorption–desorption

The BET surface area of the samples is presented in Table 1. GO showed a low BET surface area (65 m^2/g). GO sheets which were synthesized by the improved

Table 1 Physicochemical properties of the synthesized materials	Samples	N (wt%)	BET (m^2/gr)
	RGO	–	399
	NRGO500	2.4	465
	NRGO900	4.4	545
	ANRGO900	1.5	527
	RGO900	–	505
	Pd/RGO	–	263
	Pd/NRGO500	2.4	333
	Pd/NRGO900	4.4	412
	Pd/ANRGO900	1.5	390

hummers' method are aggregated when water is removed during pretreatment under vacuum conditions. Also, with the thermal expansion of GO, RGO surface area (399 m^2/g) increased because of the larger spacing between layers and smaller number of graphene layers on top of each other. In addition, according to the results, the specific surface area of the supports improves with increased nitrogen content, due to higher temperature doping, which is attributed to the formation of three-dimensional structure of NRGO [28].

As reported in Table 1, the highest BET surface area (545 m^2/g) was obtained for NRGO900 sample. In order to investigate the contribution of N-doping and temperature, RGO900 was synthesized according to the NRGO900 synthesis method without having ammonia gas atmosphere in the furnace. RGO900 showed a lower specific surface area as compared to NRGO900. Therefore, according to the results, both temperature and N-doping have contributions on enhancing the specific surface area of the samples [29].

Also, the specific surface area of catalysts decreases in the course of their synthesis within the aqueous solution. As was mentioned earlier, the supports are synthesized in the gaseous phase and lose most of their oxygen-containing groups. When they are located in the aqueous solution for deposition of active phase, they became hydrophobic to some extent, and therefore, some graphene sheets stack on top of each other that results in a reduction in surface area up to about 35% [30].

FESEM

FESEM imaging was performed on RGO and NRGO samples to elaborate on their morphology. As is observed in Fig. 1, the two-dimensional sheets are enclosed in graphene oxide, but they are disintegrated and wrinkled after expansion. By N-doping at different temperatures, more porosity is induced due to heat treatment and presence of nitrogen. One of the challenges in graphene applications in heterogeneous catalysts is the low surface area which is mostly due to shrinking and stacking of the sheets. Based on the results of this study, this challenge may be overcome to some extent is to apply heat treatment along with N-doping in order to synthesis three-dimensional structures.

Figure 1 reveals that NRGO samples have three-dimensional structures, whereas in the RGO sample synthesized under similar conditions the graphene sheets are not expanded so much [31]. Therefore, the presence of nitrogen in the structure leads to better expansion, which in turn contributes to larger specific surface area.

Raman

Raman spectra of the RGO and NRGO samples are presented in Fig. 2. RGO sample shows two evident peaks at 1350 and 1585 cm^{-1}, which are attributed to D- and G-band, respectively [32]. It is believed the G-band is indicative of sp^2 hybridization and D-band shows structural defects of the samples [28]. The spectra reveal that the structural defects increase upon N-doping, i.e., I_D/I_G increases. This increase is more obvious for NRGO900 and ANRG900 samples.
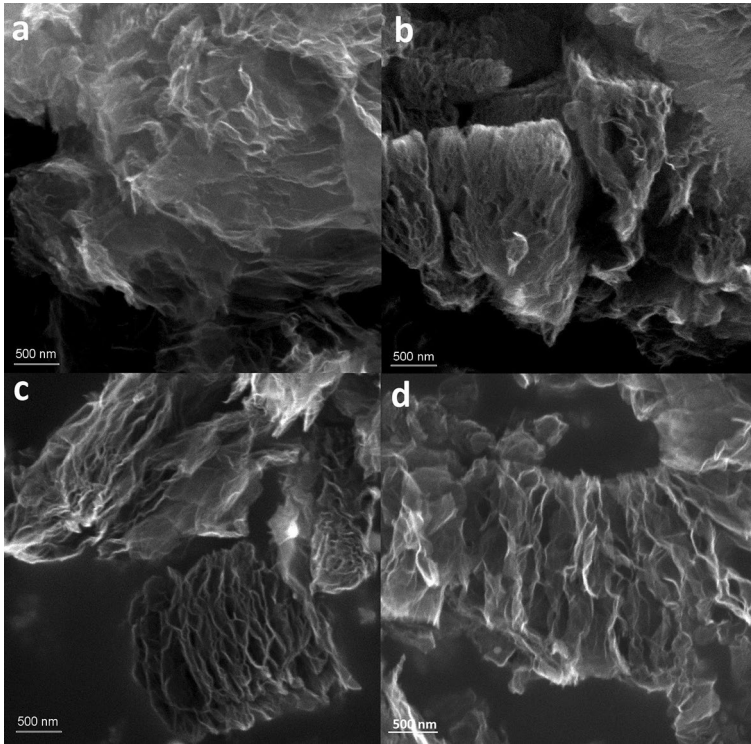
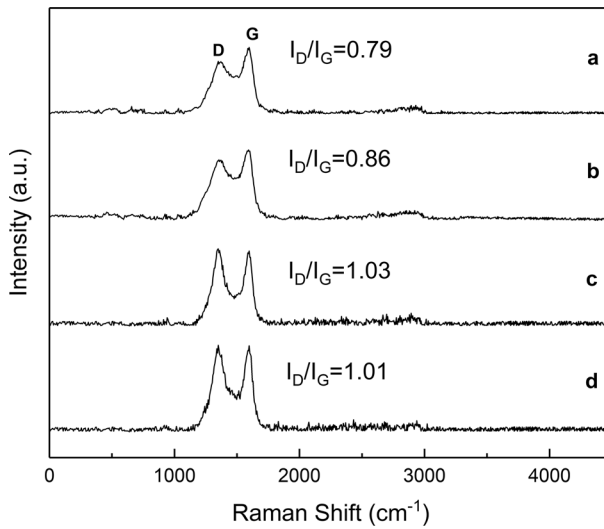**Fig. 1** FESEM images of RGO (**a**), (**b**) NRGO500, (**c**) NRGO900, and (**d**) ANRGO900

Fig. 2 Raman spectra of (**a**) RGO, (**b**) NRGO500, (**c**) ANRGO900, and (**d**) NRGO900

XPS

According to Fig. 3, the N1s peaks around 398 (pyridinic-N), 400 (pyrrolic-N), and 401 eV (graphitic-N) are related to the main types of nitrogen. These results are consistent with previous reports concerning the XPS analysis of N-doping. Since the catalyst support was annealed, the ratio of pyridinic to graphitic nitrogen appears to decrease. It is because the pyridinic-N is not stable at high temperature and is converted to other forms of nitrogen groups. The N_P/N_G is about 9 for NRGO500 sample. This ratio is suppressed to 1.8 after annealing for ANRGO900. The high ratio of N_P/N_G is thought to be responsible for enhancement of the catalytic activity [33].

Temperature-programmed desorption (TPD)

The TPD spectra of various nitrogen-doped samples are shown in Fig. 4. The effluent from the TPD reactor was analyzed continuously by a FTIR equipment. These gases are products of decomposition and elimination of oxygen-containing groups of the samples. The strength of carbon–oxygen bond is larger than that of carbon–carbon; therefore, the samples, i.e., NRGO500, NRGO900, and ANRGO900, were heated in the presence of helium gas and abstraction of the oxygen-containing groups mostly from the carbon side led to the formation of CO, and CO2 [34].

According to the previous reports [35, 36], the amount of effluent gases during TPD experiment is proportional to the amount of oxygen-containing groups and the oxygen-containing groups leading to CO2 production have lower thermal stability than the groups that are converted to CO. According to the results presented in Fig. 4, the amount of oxygen functional groups in NRGO500 was higher than
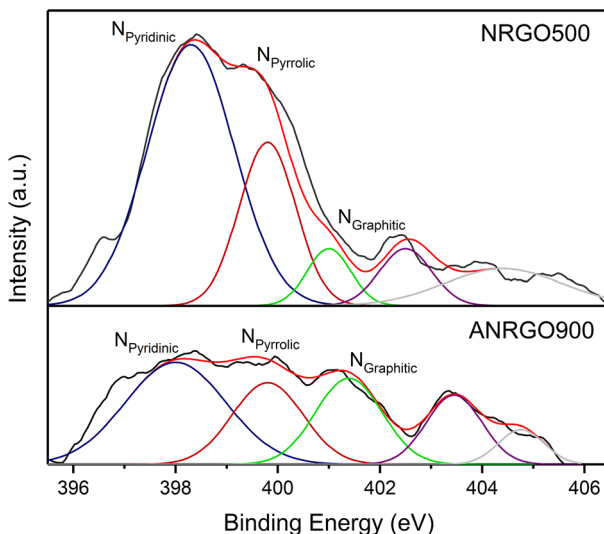

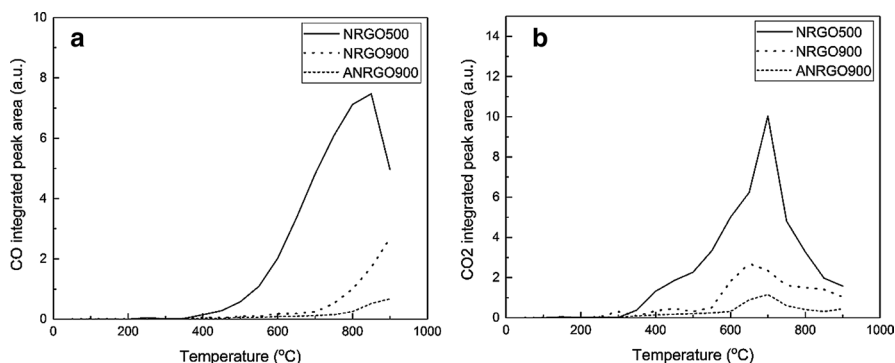**Fig. 3** XPS spectra of N1s for NRGO500 and ANRGO900 samples

Fig. 4 (**a**) CO and (**b**) CO2 variation during desorption of NRGO500, NRGO900, and ANRGO900

NRGO900 and ANRGO900. Also, due to the longer exposure to high temperature, the amount of oxygen functional groups in ANRGO900 was lower than NRGO900.

Temperature-programmed reduction (TPR)

The acquired TPR spectra for the support and Pd-containing catalysts are presented in Fig. 5, 6. As is evident in Fig. 5, the TPR spectrum for the NRGO, the high-temperature peak (higher than 350 °C) may be attributed to the support. It should be noted that the effluent from the TPR analyzer was sent to FTIR. This way, CO, CO_2, and CH_4 are detected for the TPR experiments of the supports. These products are formed due to the surface detachment and decomposition of function groups, e.g., OH groups and carbon-containing groups [37, 38].

The TPR spectrum of Pd/NRGO500 shows a sharp and strong reduction peak at 143 °C (Fig. 6). For the other samples, various broad peaks are observed due to broad size distribution of palladium species. The results present a reduction peak between 100 and 200 °C, which is ascribed to the reduction of small PdO species.
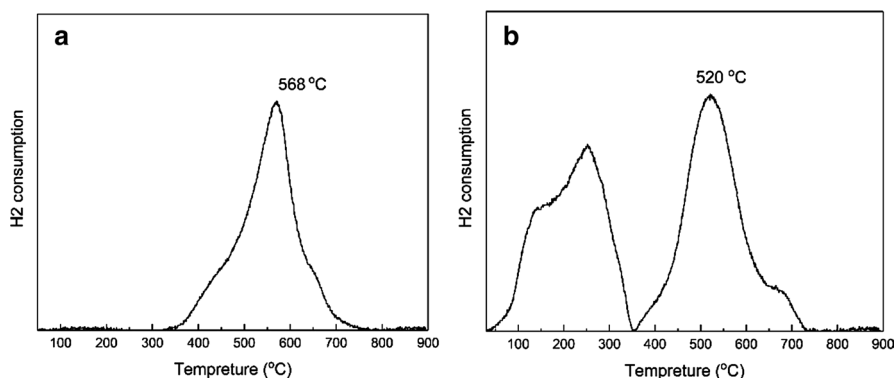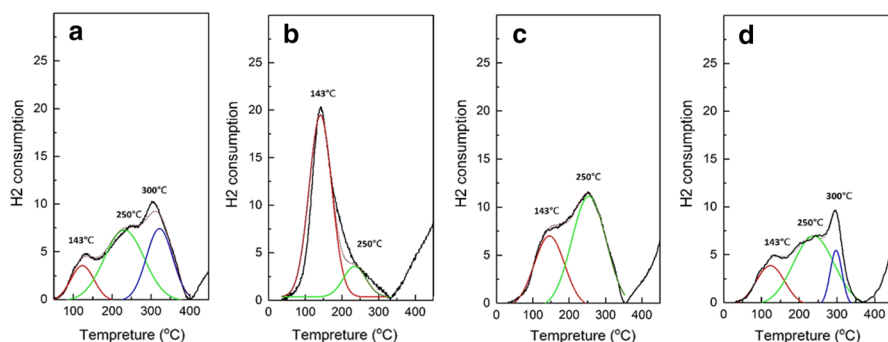

Fig. 5 TPR patterns of (**a**) NRGO900, and (**b**) Pd/NRGO900

Fig. 6 TPR profiles of (**a**) Pd/RGO, (**b**) Pd/NRGO500, (**c**) Pd/NRGO900, and (**d**) Pd/ANRGO900

Another reduction peak observed in the temperature range of 200–350 °C is attributed to the reduction of PdO particles strongly interacting with the surface of the support [39].

Total hydrogen consumption for the catalysts was calculated by integrating the area under the whole spectrum and also for the peaks centered in a designated temperature. The results are reported in Table 2. Based on the Pd loading of the samples and the required hydrogen for its reduction to metallic Pd, the H_2 consumption is higher than expected for the reduction of palladium oxide. This could be due to spillover of hydrogen to the support species located very close to the active phase [40, 41]. As was described, the H_2 consumption was calculated separately for each peak. It is evident that the Pd/NRGO500 catalyst was much more uniform than other catalysts due to the H_2 consumption at a single temperature, i.e., 143 °C.

According to the TPR results, the catalysts were reduced at different temperatures of 100, 250, and 400 °C for 2 h under H_2 flow, and their activities were evaluated for the hydrogenation of CMA under similar conditions. Catalyst reduction at 100 and 400 °C showed lower conversion than those reduced at 250 °C. Therefore, 250 °C was selected as the optimum temperature for reduction in order to measure the catalytic performance of the catalysts.

CO chemisorption

The results of CO chemisorption are presented as dispersion and Pd average particle size in Table 3. Owing to the significant aggregation of Pd/RGO, a notably small Pd

Table 2 Reduction temperatures and H_2 consumption amounts for Pd-containing catalysts with 4.5 wt% Pd loading

Samples	H_2 consumption (mmol H_2/g)			
	Total	143 °C	250 °C	300 °C
Pd/RGO	0.76	0.09	0.37	0.24
Pd/NRGO500	0.75	0.66	0.14	–
Pd/NRGO900	0.82	0.27	0.51	–
Pd/ANRGO900	0.62	0.17	0.3	0.13

Table 3 Pd average particle size and dispersions of Pd NPs

Samples	Total CO uptake (mmol CO/g)	D (%)	dp (nm)
Pd/RGO	0.00653	2.5	44
Pd/NRGO500	0.0523	20	6
Pd/NRGO900	0.0133	5.1	22
Pd/ANRGO900	0.00627	2.4	46

dispersion of 2.5% is observed. One of the main purposes of N-doping in the structure of RGO is to stabilize the palladium particles which in turn prevents their size to increase. This way the dispersion of palladium particles remains relatively high. Although Pd/ANRGO900 sample has 1.5% nitrogen in its structure, its Pd dispersion is almost similar to that of Pd/RGO catalyst. It seems that the long exposure of this sample to high temperature, i.e., 900 °C, and reduction of oxygen-containing groups are the main causes of size increase in the Pd particles. Upon long exposure to high temperatures, nitrogen atoms in the structure of RGO are changed mostly to N-graphitic structure, in which each nitrogen atom is attached to three carbon atoms. This way the nitrogen atoms are more stable and therefore cannot stabilize the Pd particles to a large extent [42].

As is shown in Table 3, the CO uptake and dispersion of Pd particles in Pd/NRGO500 are higher than those for Pd/NRGO900 particles. It appears that the presence of oxygen-containing groups adjacent to the nitrogen groups and formation of more pyridinic nitrogens than graphitic nitrogen, formed at lower temperatures, is the reason for Pd particles deposited on NRGO500 surface to be more stable and therefore less prone to sintering [43, 44].

Graphitic nitrogen in graphene structure uses four valence electrons to form σ and π bonds, and the fifth electron is in the higher energy π^* state, leading to the electron donor behavior of the support. Due to the synthesis method, i.e., incipient wetness impregnation, and the use of H_2PdCl_4 precursor, the palladium source was presented in the synthesis solution in the form of $[PdCl_4]^{2-}$. Pyridinic nitrogen with electron acceptor properties can probably cause the adsorption of charged metal ions $[PdCl_4]^{2-}$ which are deposited following the addition of $NaBH_4$ during synthesis. As a result, due to the higher ratio of pyridinic nitrogen to graphitic nitrogen in NRGO500, palladium dispersion occurs more efficiently in Pd/NRGO500 [45].

HRTEM

The HRTEM micrographs of Pd/NRGO500 catalyst are presented in Fig. 7. In Fig. 7, the morphology of graphene, Pd distribution on the surface, the lattice fringe of Pd, and distribution of Pd particle size are shown. Figure 7b indicates the proper dispersion of the Pd particles onto NRGO surface. Figure 7c shows a high-resolution TEM image of Pd particles on graphene sheets. In order to measure the particle size distribution, a population of particles was considered in different parts of the image, the size of particles was measured, and the size distribution was attained
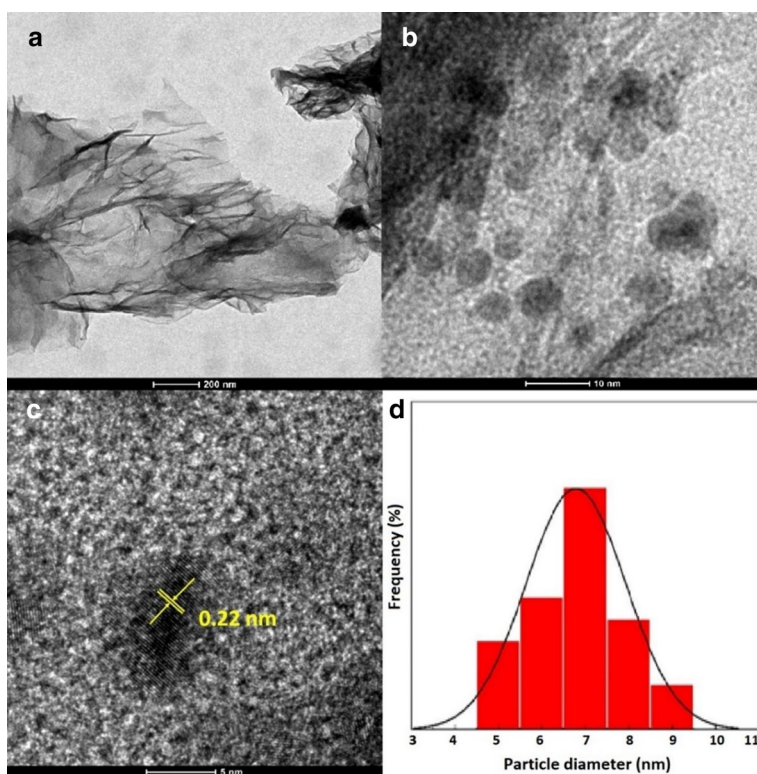
Fig. 7 HRTEM micrographs of graphene sheets (**a**), Pd particles on NRGO500 (**b**), images with increasing magnifications (lattice fringe) (**c**), particle size distribution (**d**)

accordingly (Fig. 7d). As is evident from Fig. 7d, the Pd nanoparticle sizes are in the range of 5–9, nm in a fairly good agreement with the CO chemisorption results (Table 3).

Catalytic activity

The detailed results of hydrogenation of CMA are presented in Table 4. Conversion and selectivity of the reaction for formation of HCMA demonstrate the effectiveness of nitrogen-containing functional groups in the graphene structure. In order to compare the effects of different nitrogen species in the support structure, three different catalysts were investigated, i.e., Pd/NRG500, Pd/NRGO900, and Pd/ANRGO900. The Pd/NRG500 catalyst showed the best performance among the catalysts with 98% conversion and 96% selectivity into HCMA under optimum conditions. The Pd/NRGO900 catalyst, although had nitrogen content of about twice of the corresponding content of Pd/NRGO500 catalyst, showed much less conversion, i.e., 59%. Furthermore, Pd/ANRGO900 catalyst showed similar activity to Pd/RGO despite the fact that it had 1.5% nitrogen in its structure. Therefore, the presence of nitrogen

Table 4 Comparison of the catalytic activities in hydrogenation of CMA

Catalyst	N (wt%)	D (%)	H_2 pressure (MPa)	Temperature (°C)	Time (hr)	Conv (%)	HCMA selectivity (%)
NRGO500	2.4	–	2	90	1	0	0
Pd/RGO	–	2.5	2	90	1	12	89
Pd/ANRGO900	1.5	2.4	2	90	1	12	94
Pd/NRGO900	4.2	5.1	2	90	1	59	94
Pd/NRGO500	2.4	20	2	90	1	98	96
Pd/NRGO500			2	80	1	71	94
Pd/NRGO500			2	70	1	43	92
Pd/NRGO500[a]			2	90	1	90	94
Pd/NRGO500			2	90	1.5	99 >	92

[a]The fourth run was performed to test the reusability of catalyst

or even more nitrogen in the graphene structure does not guarantee the improvement in the catalytic performance. It appears that in addition to the nitrogen presence, the type of nitrogen species in the graphene structure may have more contribution in improving the catalytic hydrogenation performance of the catalyst [46].

As explained in Sect. 2.1.6, the Pd/NRGO500 catalyst had higher H_2 consumption for reduction at lower temperatures compared to the other two catalysts. The peak of H_2 consumption designated to 143 °C in Table 2 was directly related to the performance of the catalysts. H_2 consumption at higher temperatures is indicative of a strong interaction between Pd and the support, and thus, the active phase shows less catalytic activity [39]. Since the deposition of the active phase on the support was carried out with the same method, the effect of the type of support in these catalysts is quite substantial. Therefore, it may be concluded that the improvement in the catalytic performance arises mostly due to the presence of nitrogen in the support structure and more importantly due to the type of nitrogen species of the support.

It has been reported that the catalyst activity and selectivity for C=C bond hydrogenation depend on the size of catalyst active phase to a large extent [9]. According to the results reported [47, 48], the CMA conversion increased with the decrease in the palladium particle size. As is shown in Table 4, the catalytic activity improves significantly with an increase in Pd dispersion. In order to compare the catalysts more precisely, the TOF for formation of HCMA under the same operating conditions, i.e., T and P, was calculated (Fig. 8). The Pd/NRGO500 catalyst performed much better than the other catalysts (TOF = 2 S^{-1}). Similar results have been reported by other research group [49].

As described earlier, nitrogen present in the graphene structure has an important role in performance of the catalysts, i.e., activity and selectivity. The catalysts doped with nitrogen showed selectivity to HCMA well above 90%. According to previous studies [50], the interaction between C=O group and N species on support surface in the course of reaction leads to the C=O group of CMA to stay away from Pd particles on the surface, and this way C=O hydrogenation does not occur significantly.
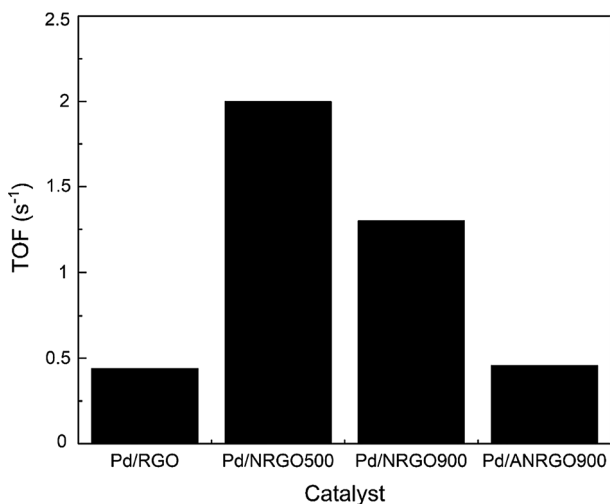
Fig. 8 Comparison of TOF of Pd-based catalysts (4.5 wt%) for hydrogenation reaction. Operating conditions: *T*: 90 °C, H$_2$ Pressure: 2 Mpa, catalyst amount: 50 mg, CAL: 4 mmol

However, increased reaction time from 1 to 1.5 h decreased the selectivity into HCMA. This seems to longer presence of HCMA in the reaction medium, which leads to the reduction of the C=O group and conversion of HCMA to HCMO.

In addition, the hydrogenation of CMA was performed at 70, 80, and 90 °C and 2 MPa hydrogen pressure on the Pd/NRGO500 catalyst. The other reaction conditions remained unchanged (Table 4). The higher temperature (90 °C) led to higher conversions and selectivity in this reaction. According to the results reported, C=C is more active than C=O at higher temperatures, i.e., thermodynamically more favorable, to account for the higher selectivity to HCMA [51]. In order to determine the activation energy of the hydrogenation reaction, a set of experiments was performed over Pd/NRGO500. By plotting the Arrhenius plot, the activation energy was calculated to be 59 kJ/mol, indicating that the results obtained were in the absence of mass transfer limitation and in the range of reported values [52].

The stability of the Pd/NRGO500 catalyst was studied through four consecutive tests at the same operating conditions. The results are presented in Fig. 9. The conversion of CMA declined slightly from 98 to 90%, while the selectivity to HCMA remained constant at a very high level of 94%, demonstrating that Pd/NRGO500 presents relatively high stability. The loss of catalytic activity is generally attributed to the interaction between Pd and supports and the aggregation of Pd nanoparticles [53].
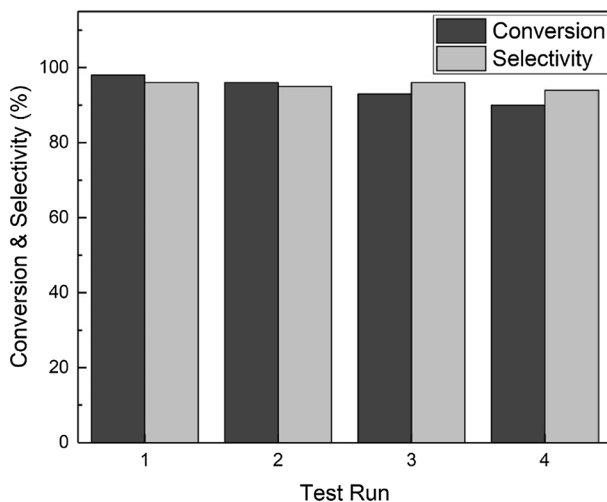
Fig. 9 Catalytic activity in four consecutive runs over Pd/NRGO500 catalyst. Reaction condition: 90 °C, H_2 pressure 2 Mpa, 1 h, catalyst amount 50 mg, CAL 4 mmol

Conclusion

Graphene supports were synthesized and exposed to nitrogen at different temperatures in order to dope the graphene with various nitrogen species in the structure of the support. The supports were impregnated with palladium and characterized with various methods. The catalysts were used for selective hydrogenation of CMA to HCMA. The results showed that the N-doping at different temperatures affects not only on the nitrogen content but also the type of nitrogen species of the support. The results of CO chemisorption, H_2-TPR, and catalytic activity indicated that Pd/NRGO500 (2.4% N) was more active than NRGO900 (4.4% N). This observation led us to conclude that the higher ratio of pyridinic nitrogen to graphitic nitrogen in Pd/NRGO500 plays the crucial role in enhanced dispersion of Pd NPs, which in turn results in high catalytic activity of CMA, high selectivity to HCMA, and more stability of palladium without significant loss in catalytic activity with time on stream.

References

1. P. Gallezot, D. Richard, Catal. Rev. **40**, 81 (1998)
2. J. Hájek, P. Kačer, V. Hulínský, L. Červený, D.Y. Murzin, Res. Chem. Intermed. **32**, 795 (2006)
3. P. Mäki-Arvela, J. Hájek, T. Salmi, D.Y. Murzin, Appl. Catal. A Gen. **292**, 1 (2005)
4. S. Wei, Y. Zhao, G. Fan, L. Yang, F. Li, Chem. Eng. J. **322**, 234 (2017)
5. G.R. Bertolini, C.I. Cabello, M. Muñoz, M. Casella, D. Gazzoli, I. Pettiti, G. Ferraris, J. Mol. Catal. A Chem. **366**, 109 (2013)
6. C.M. Piqueras, V. Puccia, D.A. Vega, M.A. Volpe, Appl. Catal. B Environ. **185**, 265 (2016)
7. J.P. Breen, R. Burch, J. Gomez-Lopez, K. Griffin, M. Hayes, Appl. Catal. A Gen. **268**, 267 (2004)
8. M. Ahmadi, H. Mistry, B.R. Cuenya, J. Phys. Chem. Lett. **7**, 3519 (2016)
9. F. Jiang, J. Cai, B. Liu, Y. Xu, X. Liu, RSC Adv. **6**, 75541 (2016)
10. X. Wang, X. Liang, P. Geng, Q. Li, ACS Catal. **10**, 2395 (2020)
11. A.S. Nagpure, L. Gurrala, P. Gogoi, S.V. Chilukuri, RSC Adv. **6**, 44333 (2016)

12. C. Hu, T. Lu, F. Chen, R. Zhang, J. Chinese Adv. Mater. Soc. **1**, 21 (2013)
13. Q. Zhao, D. Chen, Y. Li, G. Zhang, F. Zhang, X. Fan, Nanoscale **5**, 882 (2013)
14. I. Ziccarelli, H. Neumann, C. Kreyenschulte, B. Gabriele, M. Beller, Chem. Commun. **52**, 12729 (2016)
15. Y. Chen, X. Li, Z. Wei, S. Mao, J. Deng, Y. Cao, Y. Wang, Catal. Commun. **108**, 55 (2018)
16. Y. Wu, S. Chen, X. Guo, J. Wu, B. Peng, Z. Liu, Res. Chem. Intermed. **43**, 3677 (2017)
17. H. Wang, T. Maiyalagan, X. Wang, ACS Catal. **2**, 781 (2012)
18. L. Wu, Y. Long, J. Ma, G. Lu, Res. Chem. Intermed. **45**, 3809 (2019)
19. L. He, F. Weniger, H. Neumann, M. Beller, Angew. Chemie Int. Ed. **55**, 12582 (2016)
20. W.S. Hummers, R.E. Offeman, J. Am. Chem. Soc. **80**, 1339 (1958)
21. H.L. Poh, F. Šaněk, A. Ambrosi, G. Zhao, Z. Sofer, M. Pumera, Nanoscale **4**, 3515 (2012)
22. Q. Wang, X. Cui, J. Chen, X. Zheng, C. Liu, T. Xue, H. Wang, Z. Jin, L. Qiao, W. Zheng, RSC Adv. **2**, 6245 (2012)
23. S.S. Mohire, G.D. Yadav, Ind. Eng. Chem. Res. **57**, 9083 (2018)
24. M. Davoodpour, R. Tafreshi, A.A. Khodadadi, Y. Mortazavi, Korean J. Chem. Eng. **34**, 681 (2017)
25. M.J. Martínez-Ortiz, M.A. de la Rosa-Guzmán, J.R. Vargas-García, J.L. Flores-Moreno, N. Castillo, A. Guzmán-Vargas, S. Morandi, R.M. Pérez-Gutiérrez, Can. J. Chem. Eng. **96**, 297 (2017)
26. S.R. Kelemen, M. Afeworki, M.L. Gorbaty, P.J. Kwiatek, M.S. Solum, J.Z. Hu, R.J. Pugmire, Energy Fuels **16**, 1507 (2002)
27. R. Arrigo, M.E. Schuster, Z. Xie, Y. Yi, G. Wowsnick, L.L. Sun, K.E. Hermann, M. Friedrich, P. Kast, M. Hävecker, A. Knop-Gericke, R. Schlögl, ACS Catal. **5**, 2740 (2015)
28. P. Liu, G. Li, W.T. Chang, M.Y. Wu, Y.X. Li, J. Wang, RSC Adv. **5**, 72785 (2015)
29. K. Chizari, I. Janowska, M. Houllé, I. Florea, O. Ersen, T. Romero, P. Bernhardt, M.J. Ledoux, C. Pham-Huu, Appl. Catal. A Gen. **380**, 72 (2010)
30. S. Gadipelli, Z.X. Guo, Prog. Mater. Sci. **69**, 1 (2015)
31. S. Zhang, Y. Chen, Y. Yang, M. Yu, D. Liu, B. Xie, W. Yu, Y. Zhang, L. Lu, RSC Adv. **7**, 15293 (2017)
32. J. Bin Wu, M.L. Lin, X. Cong, H.N. Liu, P.H. Tan, Chem. Soc. Rev. **47**, 1822 (2018)
33. Z. He, B. Dong, W. Wang, G. Yang, Y. Cao, H. Wang, Y. Yang, Q. Wang, F. Peng, H. Yu, ACS Catal. **9**, 2893 (2019)
34. H.P. Boehm, Carbon N. Y. **40**, 145 (2002)
35. Q.L. Zhuang, T. Kyotani, A. Tomita, Carbon N. Y. **32**, 539 (1994)
36. M.V. Naseh, A.A. Khodadadi, Y. Mortazavi, F. Pourfayaz, O. Alizadeh, M. Maghrebi, Carbon N. Y. **48**, 1369 (2010)
37. E. Esmaeili, A.M. Rashidi, A.A. Khodadadi, Y. Mortazavi, M. Rashidzadeh, Fuel Process. Technol. **120**, 113 (2014)
38. S. Gil, J.M. Garcia-Vargas, L.F. Liotta, G. Pantaleo, M. Ousmane, L. Retailleau, A. Giroir-Fendler, Catalysts **5**, 671 (2015)
39. A. Aznárez, A. Gil, S.A. Korili, RSC Adv. **5**, 82296 (2015)
40. A. Cabiac, T. Cacciaguerra, P. Trens, R. Durand, G. Delahay, A. Medevielle, D. Plée, B. Coq, Appl. Catal. A Gen. **340**, 229 (2008)
41. A.L.D. Ramos, P. da Silva Alves, D.A.G. Aranda, M. Schmal, Appl. Catal. A Gen. **277**, 71 (2004)
42. D.A. Bulushev, M. Zacharska, E.V. Shlyakhova, A.L. Chuvilin, Y. Guo, S. Beloshapkin, A.V. Okotrub, L.G. Bulusheva, ACS Catal. **6**, 681 (2016)
43. J. Huo, P. Duan, H.N. Pham, Y.J. Chan, A.K. Datye, K. Schmidt-Rohr, B.H. Shanks, Catal. Sci. Technol. **8**, 3548 (2018)
44. L. Lai, J.R. Potts, D. Zhan, L. Wang, C.K. Poh, C. Tang, H. Gong, Z. Shen, J. Lin, R.S. Ruoff, Energy Environ. Sci. **5**, 7936 (2012)
45. X. Ning, H. Yu, F. Peng, H. Wang, J. Catal. **325**, 136 (2015)
46. M. Megawati, C.K. Chua, Z. Sofer, K. Klímová, M. Pumera, Phys. Chem. Chem. Phys. **19**, 15914 (2017)
47. S. Ashokkumar, V. Ganesan, K.K. Ramaswamy, V. Balasubramanian, Res. Chem. Intermed. **44**, 6703 (2018)
48. S. Cattaneo, F. J. S. Trujillo, N. Dimitratos, and A. Villa, Appl. Sci. **9**, (2019).
49. F. Wang, Z. Zhang, X. Wei, Q. Fang, X. Jiang, Appl. Catal. A Gen. **543**, 196 (2017)
50. R. Nie, M. Miao, W. Du, J. Shi, Y. Liu, Z. Hou, Appl. Catal. B Environ. **180**, 607 (2016)
51. K.J.A. Raj, M.G. Prakash, T. Elangovan, B. Viswanathan, Catal. Lett. **142**, 87 (2012)
52. H.A. Ali, M.Z. Al-Noaimi, S.S. Mahmoud, Jordan J. Chem. **10**, 58 (2015)
53. S. Cattaneo, S.J. Freakley, D.J. Morgan, M. Sankar, N. Dimitratos, G.J. Hutchings, Catal. Sci. Technol. **8**, 1677 (2018)